

# Wave function of $2S$ radially excited vector mesons from data for diffraction slope

J. Nemchik

*Institute of Experimental Physics, Slovak Academy of Sciences, Watsonova 47, 04353 Košice, Slovakia*

(Received 24 May 2000; published 5 March 2001)

In color dipole generalized Balitskiĭ-Fadin-Kuraev-Lipatov dynamics, we predict a strikingly different  $Q^2$  and energy dependence of the diffraction slope for the diffractive production of ground state  $V(1S)$  and radially excited  $V'(2S)$  light vector mesons. The color dipole model predictions for the diffraction slope for  $\rho^\circ$  and  $\phi^\circ$  production are in a good agreement with the data from the fixed target and collider DESY HERA experiments. We present how a different pattern of anomalous energy and  $Q^2$  dependence of the diffraction slope for  $V'(2S)$  production leads to a different position of the node in the radial wave function. We discuss how to determine this node position from the fixed target and HERA data.

DOI: 10.1103/PhysRevD.63.074007

PACS number(s): 13.60.Hb, 13.60.Le

## I. INTRODUCTION

Diffractive photoproduction and electroproduction of vector mesons

$$\gamma^* p \rightarrow V p \quad (V = \rho^0, \Phi^0, \omega^0, J/\Psi, Y, \dots) \quad (1)$$

is presently intensively studied at the DESY  $ep$  collider HERA and represents a good cross check to test the ideas implemented in various theoretical models [1–9] within the framework of the perturbative QCD (PQCD). Moreover, the high statistics data at HERA during recent years allow us also to study the diffractive electroproduction of radially excited  $V'(2S)$  vector mesons, which are known to have a node in the radial wave function leading to a lot of peculiarities in the investigation of various aspects of their diffractive production. The new data especially for  $V'(2S)$  light vector mesons obtained at HERA can help to distinguish between various theoretical models and also to determine a relative sign of  $V(1S)$  and  $V'(2S)$  production amplitudes.

The details of the generalized Balitskiĭ-Fadin-Kuraev-Lipatov (GBFKL) phenomenology of diffractive electroproduction of vector mesons has been presented in the paper [10] and need not be repeated here. The same reason concerns the color dipole phenomenology of the diffraction slope developed in the paper [11]. Vector meson production is quantified in the mixed  $(\mathbf{r}, z)$  light-cone technique [12,13]. High-energy hadrons and photons are treated as systems of color dipoles with the transverse size  $\mathbf{r}$ . Interaction of color dipoles with the target nucleon is quantified by the color dipole cross section  $\sigma(\xi, r)$ , where  $\xi = \log[(W^2 + Q^2)/(m_V^2 + Q^2)]$  is the rapidity variable at c.m.s. energy  $W$ . Energy evolution of  $\sigma(\xi, r)$  is described by the generalized BFKL equation [13,14]. The principal result coming from the analysis of the diffractive production of light [6,10] and heavy [11] vector mesons at  $t=0$  within the GBFKL phenomenology leads to the conclusion that the  $V(1S)$  vector meson production amplitude probes the color dipole cross section (and the dipole diffraction slope as well) at the dipole size  $r \sim r_S$  (scanning phenomenon [15,4–6]), where the scanning radius can be expressed through the scale parameter  $A$ , photon virtuality  $Q^2$ , and vector meson mass  $m_V$ :

$$r_S \approx \frac{A}{\sqrt{m_V^2 + Q^2}}. \quad (2)$$

Scanning phenomenon connects the shrinkage of the photon with  $Q^2$  together with  $\sim r^2$  behavior of the dipole cross section at small  $r$ . The scanning phenomenon allows us to study the transition between the perturbative (hard) and nonperturbative (soft) regimes. Changing  $Q^2$  and the mass of the produced vector meson one can probe the dipole cross section  $\sigma(\xi, r)$  in a very broad range of the dipole sizes  $r$ . Furthermore, the scanning radius defines the transverse size of  $\gamma^* V$  transition vertex, which contributes to diffraction slope  $B(\gamma^* \rightarrow V)$ .

Diffractive production of radially excited  $V'(2S)$  vector mesons can provide additional information on the dipole cross section and the dipole diffraction slope. The presence of the node in  $V'(2S)$  radial wave function leads to the node effect [2,15,16,10,11,17]  $Q^2$  and energy dependent strong cancellation of contributions to the production amplitude from dipole sizes larger and smaller than the node position  $r_n$  in  $V'(2S)$  radial wave function. The onset of the node effect depends also on the vector meson mass. The lighter the vector meson the stronger the node effect. A very strong node effect has been studied in electroproduction of radially excited light vector mesons ( $\rho^\circ, \phi^\circ, \omega^\circ$ ) leading to a very spectacular pattern of anomalous  $Q^2$  and energy dependence of production cross section [10]. The node effect is much weaker for electroproduction of  $\Psi'(2S)$  vector mesons. However, it still leads to a slightly different  $Q^2$  and energy dependence of production cross section for  $\Psi'$  vs  $J/\Psi$  and to a counterintuitive inequality  $B(\Psi') < B(J/\Psi)$  [11]. For  $Y'$  production the node effect is negligibly small and gives approximately the same  $Q^2$  and energy behavior of production cross section and practically the same diffraction slope as for  $Y$  production [11]. Another demonstration of the node effect concerns to the  $V'(2S)/V(1S)$  production ratio resulting in a strong suppression of diffraction production  $V'(2S)$  vs  $V(1S)$ . This result has been confirmed by the data on  $\Psi'$  and  $J/\Psi$  photoproduction at HERA and fixed target experiments. The node effect has a very interesting manifestation in differential cross section  $d\sigma/dt$  for production of  $V'(2S)$  light vector mesons leading to a very complicated pattern of

anomalous  $t$  behavior of  $d\sigma/dt$  at different  $Q^2$  and energies [17]. We found a correspondence between a specific pattern of that nonmonotonic  $t$  dependence and the position of the node in radial  $V'(2S)$  wave function. The predicted anomalies coming from the node effect can be tested at HERA.

Motivated by the above very interesting results followed from the node effect we study further the salient features of the node effect with conjunction with the GBFKL phenomenology of the diffraction slope [18,19,11]. The main emphasis is focused to the production of  $V'(2S)$  light vector mesons due to a very strong node effect. We predict a strikingly different  $Q^2$  and energy dependence of the diffraction slope for the production of  $V'(2S)$  vs  $V(1S)$  vector mesons. We find a very spectacular pattern of anomalous  $Q^2$  and energy dependence for the  $V'(2S)$  diffraction slope and analyze how the node position in the  $V'(2S)$  radial wave function can be extracted from the low-energy and HERA data. We would like to emphasize that only the color dipole GBFKL phenomenology for diffractive production of vector mesons [10,11] together with the scanning phenomenon allows us to perform such an analysis of the node position in  $V'(2S)$  radial wave function from the data for  $V'(2S)$  diffraction slope.

The paper is organized as follows. In Sec. II we present a very short review of the color dipole phenomenology of the diffractive photoproduction and electroproduction of vector mesons including some needful results from the GBFKL phenomenology of the diffraction slope. Section III contains the model predictions for  $Q^2$  and energy dependence of the diffraction slope for the  $\rho^\circ$  and  $\phi^\circ$  real and virtual electroproduction. We predict a substantial growth of the diffraction slope with energy in agreement with the low energy data and the data from the HERA collider experiments. The subject of Sec. IV refers to the anomalous  $Q^2$  and energy dependence of diffraction slope for electroproduction of  $V'(2S)$  radially excited light vector mesons. We find a correspondence between a specific pattern of nonmonotonic  $Q^2$  and energy behavior of the diffraction slope and the position of the node in  $V'(2S)$  wave function. The summary and conclusions are presented in Sec. V.

## II. BASIC FORMULAS FROM THE COLOR DIPOLE PHENOMENOLOGY OF VECTOR MESON PRODUCTION AND THE DIFFRACTION SLOPE

A very popular and powerful tool for the study of the dynamics of vector meson diffractive photoproduction and electroproduction is the light-cone representation introduced in Ref. [20]. The central point of this approach is that in the mixed  $(\mathbf{r}, z)$  representation the high-energy vector meson can be treated as a system of color dipole described by the distribution of the transverse separation  $\mathbf{r}$  of the quark and antiquark given by the  $q\bar{q}$  wave function  $\Psi(\mathbf{r}, z)$ , where  $z$  is the fraction of the meson's light-cone momentum carried by a quark. In this approach the imaginary part of the production amplitude for the real (virtual) photoproduction of vector mesons with the momentum transfer  $\mathbf{q}$  can be represented in the factorized form

$$\begin{aligned} \text{Im } \mathcal{M}(\gamma^* \rightarrow V, \xi, Q^2, \mathbf{q}) &= \langle V | \sigma(\xi, r, z, \mathbf{q}) | \gamma^* \rangle \\ &= \int_0^1 dz \int d^2\mathbf{r} \sigma(\xi, r, z, \mathbf{q}) \\ &\quad \times \Psi_V^*(\mathbf{r}, z) \Psi_{\gamma^*}(\mathbf{r}, z) \end{aligned} \quad (3)$$

whose normalization is  $d\sigma/dt|_{t=0} = |\mathcal{M}|^2/16\pi$ . In Eq. (3),  $\Psi_{\gamma^*}(\mathbf{r}, z)$  and  $\Psi_V(\mathbf{r}, z)$  represent the probability amplitudes to find the color dipole of size  $r$  in the photon and quarkonium (vector meson), respectively. The color dipole distribution in (virtual) photons was derived in Refs. [12,13].  $\sigma(\xi, r, z, \mathbf{q})$  in Eq. (3) is the dipole scattering matrix for the  $q\bar{q}-N$  interaction. At  $\mathbf{q}=0$  it represents the color dipole cross section, which quantifies the interaction of the relativistic color dipole of the dipole size  $\mathbf{r}$  with the target nucleon. The dipole cross section  $\sigma(\xi, r)$  is flavor independent and represents the universal function of  $r$  which describes various diffractive processes in unified form. The energy dependence of the dipole cross section reflects the importance of the higher Fock states  $q\bar{q}g\cdots$  at high energy  $\nu$ . In the leading-log( $1/x$ ) approximation the effect of higher Fock states can be reabsorbed into the energy dependence of  $\sigma(\xi, r)$ , which satisfies the GBFKL equation [13,14] for the energy evolution.

At the small  $\mathbf{q}$  considered in this paper, one can safely neglect the  $z$  dependence of  $\sigma(\xi, r, z, \mathbf{q})$  for light and heavy vector meson production and set  $z = \frac{1}{2}$ . This also follows from the analysis within double gluon exchange approximation [12] leading to a slow  $z$  dependence of the dipole cross section.

The energy dependence of the dipole cross section is quantified in terms of the dimensionless rapidity  $\xi = \log(1/x_{\text{eff}})$ , where  $x_{\text{eff}}$  is the effective value of the Bjorken variable

$$x_{\text{eff}} = \frac{Q^2 + m_V^2}{Q^2 + W^2} \approx \frac{m_V^2 + Q^2}{2vm_p}, \quad (4)$$

where  $m_p$  is the proton mass. Hereafter, we will write the energy dependence of the dipole cross section in both variables, either in  $\xi$  or in  $x_{\text{eff}}$ .

The production amplitudes for the transversely ( $T$ ) and the longitudinally ( $L$ ) polarized vector mesons with the momentum transfer  $\mathbf{q}$  can be written in a more explicit form [6,11]:

$$\begin{aligned} \text{Im } \mathcal{M}_T(x_{\text{eff}}, Q^2, \mathbf{q}) &= \frac{N_c C_V \sqrt{4\pi\alpha_{em}}}{(2\pi)^2} \int d^2\mathbf{r} \sigma(x_{\text{eff}}, r, \mathbf{q}) \\ &\quad \times \int_0^1 \frac{dz}{z(1-z)} \{ m_q^2 K_0(\varepsilon r) \phi(r, z) \\ &\quad - [z^2 + (1-z)^2] \varepsilon K_1(\varepsilon r) \partial_r \phi(r, z) \}, \end{aligned} \quad (5)$$

$$\begin{aligned}
 & \text{Im } \mathcal{M}_L(x_{\text{eff}}, Q^2, \mathbf{q}) \\
 &= \frac{N_c C_V \sqrt{4\pi\alpha_{em}}}{(2\pi)^2} \frac{2\sqrt{Q^2}}{m_V} \int d^2\mathbf{r} \sigma(x_{\text{eff}}, r, \mathbf{q}) \\
 & \times \int_0^1 dz \{ [m_q^2 + z(1-z)m_V^2] K_0(\varepsilon r) \phi(r, z) \\
 & - \partial_r^2 \phi(r, z) \}, \quad (6)
 \end{aligned}$$

where

$$\varepsilon^2 = m_q^2 + z(1-z)Q^2, \quad (7)$$

$\alpha_{em}$  is the fine structure constant,  $N_c=3$  is the number of colors,  $C_V=1/\sqrt{2}, 1/3\sqrt{2}, \frac{1}{3}, \frac{2}{3}, \frac{1}{3}$  for  $\rho^\circ, \omega^\circ, \phi^\circ, J/\Psi, Y$  production, respectively, and  $K_{0,1}(x)$  are the modified Bessel functions. The detailed discussion and parametrization of the light-cone radial wave function  $\phi(r, z)$  of the  $q\bar{q}$  Fock state of the vector meson is given in Ref. [10].

The terms  $\propto \varepsilon K_1(\varepsilon r) \partial_r \phi(\mathbf{r}, z)$  for (*T*) polarization and  $\propto K_0(\varepsilon r) \partial_r^2 \Phi(\mathbf{r}, z)$  for (*L*) polarization in the integrands of Eqs. (5) and (6) represent the relativistic corrections which become important at large  $Q^2$  and for the production of light vector mesons. For the production of heavy quarkonia the nonrelativistic approximation can be used with a rather high accuracy [2].

A small real part of production amplitudes is also included in the model predictions and can be taken in the form [21]

$$\text{Re } \mathcal{M}(\xi, r) = \frac{\pi}{2} \frac{\partial}{\partial \xi} \text{Im } \mathcal{M}(\xi, r). \quad (8)$$

This small correction for the real part can be easily included in the production amplitudes (5),(6) using substitution

$$\begin{aligned}
 \sigma(x_{\text{eff}}, r, \mathbf{q}) &\rightarrow \left( 1 - i \frac{\pi}{2} \frac{\partial}{\partial \log x_{\text{eff}}} \right) \sigma(x_{\text{eff}}, r) \\
 &= [1 - i\alpha_V(x_{\text{eff}}, r)] \sigma(x_{\text{eff}}, r, \mathbf{q}). \quad (9)
 \end{aligned}$$

Because of a very slow onset of the pure perturbative region [see Eq. (2)], one can easily anticipate a contribution to the production amplitude coming from the semiperturbative and nonperturbative  $r \gtrsim R_c$  ( $R_c \sim 0.27$  fm is the gluon correlation radius introduced in Refs. [13,14]). Following the simplest assumption about an additive property of the perturbative and nonperturbative mechanism of interaction, we can represent the contribution of the bare Pomeron exchange to  $\sigma(\xi, r, \mathbf{q})$  as a sum of the perturbative and nonperturbative component [10,11]

$$\sigma(\xi, r, \mathbf{q}) = \sigma_{\text{pt}}(\xi, r, \mathbf{q}) + \sigma_{\text{npt}}(\xi, r, \mathbf{q}), \quad (10)$$

with the parametrization of both components at small  $\mathbf{q}$

$$\sigma_{\text{pt,npt}}(\xi, r, \mathbf{q}) = \sigma_{\text{pt,npt}}(\xi, r, \mathbf{q}=0) \exp\left(-\frac{1}{2} B_{\text{pt,npt}}(\xi, r) \mathbf{q}^2\right). \quad (11)$$

Here  $\sigma_{\text{pt,npt}}(\xi, r, \mathbf{q}=0) = \sigma_{\text{pt,npt}}(\xi, r)$  represent the contribution of the perturbative and nonperturbative mechanism to the  $q\bar{q}$ -nucleon interaction cross section, respectively,  $B_{\text{pt,npt}}(\xi, r)$  are the corresponding diffraction slopes.

The formalism for calculation of  $\sigma_{\text{pt}}(\xi, r)$  in the leading-log *s* approximation was developed in Refs. [12–14]. The nonperturbative contribution  $\sigma_{\text{npt}}(\xi, r)$  to the dipole cross section was used in Refs. [22,6,10,11] where we assume that this soft nonperturbative component of the Pomeron is a simple Regge pole with the intercept  $\Delta_{\text{npt}}=0$ . The particular form together with assumption of the energy independent  $\sigma_{\text{npt}}(\xi=\xi_0, r) = \sigma_{\text{npt}}(r)$  ( $\xi_0$  corresponds to boundary condition for the GBFKL evolution,  $\xi_0 = \log 1/x_0$ ,  $x_0=0.03$ ) allows one to successfully describe [22] the proton structure function at very small  $Q^2$ , the real photoabsorption [6], and diffractive real and virtual photoproduction of light [10] and heavy [11] vector mesons. A larger contribution of the nonperturbative Pomeron exchange to  $\sigma_{\text{tot}}(\gamma p)$  vs  $\sigma_{\text{tot}}(\gamma^* p)$  can, for example, explain a much slower rise with energy of the real photoabsorption cross section  $\sigma_{\text{tot}}(\gamma p)$ , in comparison with  $F_2(x, Q^2) \propto \sigma_{\text{tot}}(\gamma^* p)$  observed at HERA [23,24]. In addition, the reasonable form of this soft cross section  $\sigma_{\text{npt}}(r)$  was confirmed in the process of the first determination of the dipole cross section from the experimental data on vector meson electroproduction [25]. The so extracted dipole cross section is in good agreement with the dipole cross section obtained from the GBFKL dynamics [6,22]. Consequently, this nonperturbative component of the Pomeron exchange plays a dominant role at low NMC energies in the production of the light vector mesons, where the scanning radius  $r_S$  (2) is large. However, the perturbative component of the Pomeron becomes more important at larger energies also in the nonperturbative region of the dipole sizes.

As the result of the generalization of the factorization formula (3) to the diffraction slope of the reaction  $\gamma^* p \rightarrow V p$  one can write [18,11]

$$\begin{aligned}
 & B(\gamma^* \rightarrow V, \xi, Q^2) \text{Im } \mathcal{M}(\gamma^* \rightarrow V, \xi, Q^2, \mathbf{q}=0) \\
 &= \int_0^1 dz \int d^2\mathbf{r} \lambda(\xi, r) \Psi_V^*(r, z) \Psi_{\gamma^*}(r, z), \quad (12)
 \end{aligned}$$

where

$$\lambda(\xi, r) = \int d^2\mathbf{b} \mathbf{b}^2 \Gamma(\xi, \mathbf{r}, \mathbf{b}). \quad (13)$$

Then the diffraction slope can be expressed through the amplitude  $\text{Im } \mathcal{M}$  of elastic scattering of the color dipole

$$B(\xi, r) = -2d \log \text{Im } \mathcal{M}(\xi, r, \mathbf{q}) / dq^2|_{q=0} \quad (14)$$

and also reads

$$B(\xi, r) = \frac{1}{2} \langle \mathbf{b}^2 \rangle = \lambda(\xi, r) / \sigma(\xi, r). \quad (15)$$

The amplitude  $\text{Im } \mathcal{M}(\xi, r, \mathbf{q})$  in Eq. (14) within the impact-parameter representation is expressed

$$\text{Im } \mathcal{M}(\xi, r, \mathbf{q}) = 2 \int d^2 \mathbf{b} \exp(-i \mathbf{q} \mathbf{b}) \Gamma(\xi, \mathbf{r}, \mathbf{b}), \quad (16)$$

where  $\Gamma(\xi, \mathbf{r}, \mathbf{b})$  is the profile function and  $\mathbf{b}$  is the impact parameter defined with respect to the center of the  $q\bar{q}$  dipole.

The diffraction cone in the color dipole GBFKL approach for production of vector mesons has been studied in detail in Ref. [11]. Here we only present the salient feature of the color diffraction slope reflecting the presence of the geometrical contribution from beam dipole  $r^2/8$  and the contribution from the target proton size  $R_N^2/3$ :

$$B(\xi, r) = \frac{1}{8} r^2 + \frac{1}{3} R_N^2 + 2\alpha'_p(\xi - \xi_0) + \mathcal{O}(R_c^2), \quad (17)$$

where  $R_N$  is the radius of the proton. For electroproduction of light vector mesons the scanning radius is larger than the correlation one  $r \geq R_c$  even for  $Q^2 \leq 50 \text{ GeV}^2$  and one recovers a sort of additive quark model, in which the uncorrelated gluonic clouds build up around the beam and target quarks and antiquarks and the term  $2\alpha'_p(\xi - \xi_0)$  describe the familiar Regge growth of diffraction slope for the quark-quark scattering. The geometrical contribution to the diffraction slope from the target proton size  $\frac{1}{3}R_N^2$  persists for all dipole sizes  $r \geq R_c$  and  $r \leq R_c$ . The last term in Eq. (17) is also associated with the proton size and is negligibly small.

The soft Pomeron and diffractive scattering of large color dipole has been also studied in detail in Ref. [11]. Here we assume the conventional Regge rise of the diffraction slope for the soft Pomeron

$$B_{\text{npt}}(\xi, r) = \Delta B_d(r) + \Delta B_N + 2\alpha'_{\text{npt}}(\xi - \xi_0), \quad (18)$$

where  $\Delta B_d(r)$  and  $\Delta B_N$  stand for the contribution from the beam dipole and target nucleon size. As guidance we take the experimental data on the pion-nucleon scattering [26], which suggest  $\alpha'_{\text{npt}} = 0.15 \text{ GeV}^{-2}$ . In Eq. (18) the proton size contribution is

$$\Delta B_N = \frac{1}{3} R_N^2, \quad (19)$$

and the beam dipole contribution has been proposed to have the form

$$\Delta B_d(r) = \frac{r^2}{8} \frac{r^2 + aR_N^2}{3r^2 + aR_N^2}, \quad (20)$$

where  $a$  is a phenomenological parameter  $a \sim 1$ . We take  $\Delta B_N = 4.8 \text{ GeV}^{-2}$ . Then the pion-nucleon diffraction slope is reproduced with reasonable value of the parameter  $a$  in the formula (20):  $a = 0.9$  for  $\alpha'_{\text{npt}} = 0.15 \text{ GeV}^{-2}$  [11].

Following the simple geometrical properties of the GBFKL diffraction slope  $B(\xi, r)$  [see Eq. (17) and Ref. [18]] one can express its energy dependence through the energy dependent effective Regge slope  $\alpha'_{\text{eff}}(\xi, r)$

$$B_{\text{pt}}(\xi, r) \approx \frac{1}{3} \langle R_N^2 \rangle + \frac{1}{8} r^2 + 2\alpha'_{\text{eff}}(\xi, r)(\xi - \xi_0). \quad (21)$$

The effective Regge slope  $\alpha'_{\text{eff}}(\xi, r)$  varies with energy differently at different size of the color dipole [18]; at fixed scanning radius and/or  $Q^2 + m_V^2$ , it decreases with energy. At fixed rapidity  $\xi$  and/or  $x_{\text{eff}}$  (4),  $\alpha'_{\text{eff}}(\xi, r)$  rises with  $r \leq 1.5 \text{ fm}$ . At fixed energy, it is a flat function of the scanning radius. At the asymptotically large  $\xi$  ( $W$ ),  $\alpha'_{\text{eff}}(\xi, r) \rightarrow \alpha'_p = 0.072 \text{ GeV}^{-2}$ . At the lower and HERA energies, the sub-asymptotic  $\alpha'_{\text{eff}}(\xi, r) \sim (0.15 - 0.20) \text{ GeV}^{-2}$  and is very close to  $\alpha'_{\text{soft}}$  known from the Regge phenomenology of soft scattering. This means that the GBKFL dynamics predicts a substantial rise with the energy and dipole size  $r$  of the diffraction slope  $B(\xi, r)$  in accordance with the energy and dipole size dependence of the effective Regge slope  $\alpha'_{\text{eff}}(\xi, r)$  and due to the presence of the geometrical components  $\propto r^2$  in Eq. (17) and  $\Delta B_d(r) \propto r^{1.7}$  in Eq. (18) [see also Eq. (20)].<sup>1</sup> The overall dipole diffraction slope contains contributions from both  $B_{\text{npt}}(\xi, r)$  and  $B_{\text{pt}}(\xi, r)$  and corresponding geometrical component has  $r^\alpha$  behavior with  $1.7 < \alpha \leq 2.0$  (see also Ref. [27]). Therefore, for simplicity presenting discussion on the qualitative level in the subsequent sections we assume (with quite reasonable accuracy) an approximate  $r^2$  dependence of the geometrical component contribution to the dipole diffraction slope.

For a somewhat better understanding of anomalous properties of the forward  $V'(2S)$  diffraction slope, the generalized factorization formula (12) can be rewritten as the ratio of two matrix elements

$$\begin{aligned} B[\gamma^* \rightarrow V(V'), \xi, Q^2, \mathbf{q} = 0] &= \frac{\langle V(V') | \sigma(\xi, r) B(\xi, r) | \gamma^* \rangle}{\langle V(V') | \sigma(\xi, r) | \gamma^* \rangle} \\ &= \frac{\int_0^1 dz \int d^2 \mathbf{r} \sigma(\xi, r) B(\xi, r) \Psi_{V(V')}^*(\mathbf{r}, z) \Psi_{\gamma^*}(\mathbf{r}, z)}{\int_0^1 dz \int d^2 \mathbf{r} \sigma(\xi, r) \Psi_{V(V')}^*(\mathbf{r}, z) \Psi_{\gamma^*}(\mathbf{r}, z)} \\ &= \frac{\mathcal{N}}{\mathcal{D}}, \end{aligned} \quad (22)$$

where  $\mathcal{N}$  and  $\mathcal{D}$  denotes the numerator and denominator, respectively.

<sup>1</sup>Dipole size behavior of  $\Delta B_d(r)$  (20) representing the geometrical contribution to the dipole diffraction slope  $B_{\text{npt}}(\xi, r)$  (18) for diffractive scattering of large color dipole has the standard  $r^2$  dependence at small  $r^2 \ll aR_N^2$  and large  $r^2 \gg aR_N^2$  values of dipole size, respectively. In the intermediate region  $r^2 \sim aR_N^2$ , which corresponds to production of  $V(1S)$  and  $V'(2S)$  light vector mesons, the dipole size dependence of  $\Delta B_d(r)$  can be parametrized by the power function  $r^\alpha$  with  $\alpha \sim 1.7$ .

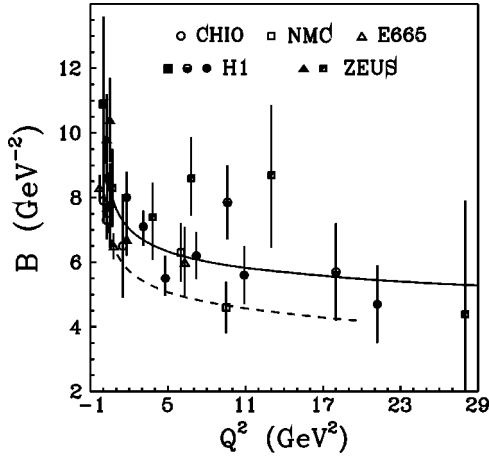


FIG. 1. The color dipole model predictions for the  $Q^2$  dependence of the diffraction slope for the production of  $\rho^0$  vs the low-energy fixed target CHIO [28], NMC [29], E665 [30] and high-energy ZEUS [34–38] and H1 [31–33] data.

### III. DIFFRACTION SLOPE FOR $\rho^0$ AND $\phi^0$ ELECTROPRODUCTION: MODEL PREDICTIONS VS EXPERIMENT

First, the model predictions for the diffraction slope will be tested taking the fixed target and HERA data for  $V(1S)$  vector meson production. The color dipole GBFKL dynamics predicts a substantial growth with energy of the diffraction slope coming from Eqs. (18) and (21). According to an approximate  $\propto r^2$  dependence of the geometrical contribution to the slope parameter [see Eqs. (18) and (21)] we expect a shrinkage of the diffraction slope with  $Q^2$  in accordance with the scanning property in vector meson production [see Eq. (2)]. In Fig. 1 we compare the model predictions for  $Q^2$  dependence of the diffraction slope for  $\rho^0$  production with the low energy data of the CHIO [28], New Muon Collaboration (NMC) [29], and E665 [30] Collaborations and the data from H1 [31–33] and ZEUS [34–38] experiments. Although the experimental data have still large error bars, they show a trend to smaller values of the diffraction slope as  $Q^2$  increases. We predict a steep shrinkage of  $B(\rho^0)$  with  $Q^2$  on the scale  $Q^2 \in (0, 5) \text{ GeV}^2$ : it falls down by  $\sim 4 \text{ GeV}^{-2}$  from  $\sim 8.7 \text{ GeV}^{-2}$  at  $Q^2=0$  down to  $5.0 \text{ GeV}^{-2}$  at  $Q^2=5 \text{ GeV}^2$  and to  $4.6 \text{ GeV}^{-2}$  at  $Q^2=10 \text{ GeV}^2$  in accordance with the low-energy CHIO, NMC, and E665 data. At HERA energy we predict a higher shrinkage from  $\sim 10.7 \text{ GeV}^{-2}$  at  $Q^2=0$  down to  $\sim 6.0 \text{ GeV}^{-2}$  at  $Q^2=10 \text{ GeV}^2$  not in disagreement with the data of H1 and ZEUS Collaborations. Concerning the shrinkage of the diffraction slope with energy  $W$ , in the photoproduction limit  $Q^2=0$  the data show the onset of the considerably large rise from the fixed target to HERA energy range. However, the large error bars of the data affect the large errors on the  $\alpha'$  fit [36] and preclude any definitive statement. In Fig. 2 we predict this substantial growth by  $\sim 2.3\text{--}2.4 \text{ GeV}^{-2}$  from  $\sim 8.3\text{--}8.4 \text{ GeV}^{-2}$  at  $W=10 \text{ GeV}$  up to  $\sim 10.7 \text{ GeV}^{-2}$  at  $W=100 \text{ GeV}$  in accordance with the data from the fixed target experiments [39] and the data from HERA experiments [31,34–36]. This rise corresponds to an effective Regge slope  $\alpha' \sim 0.25\text{--}0.26 \text{ GeV}^{-2}$ .

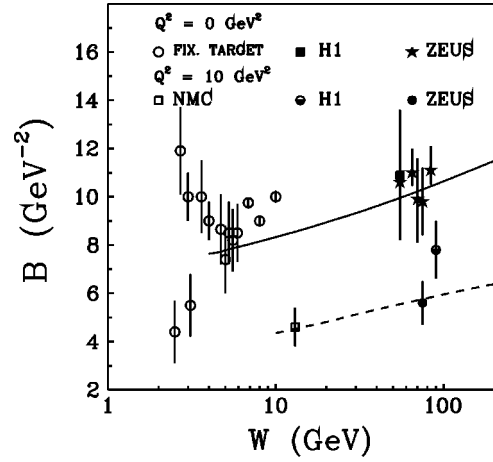


FIG. 2. The color dipole model predictions for the  $W$  dependence of the diffraction slope for the production of  $\rho^0$  vs the low-energy fixed target [39,29], and high-energy ZEUS [34–36] and H1 [31–33] data. The top solid curve is a prediction for the diffraction slope at  $Q^2=0$ . The lower dashed curve represents a prediction at  $Q^2=10 \text{ GeV}^2$ .

We would like to emphasize that the overall effective Regge slope  $\alpha'$  contains the energy dependent contribution of the perturbative component  $\alpha'_{\text{eff}}(\xi, r)$  characterizing the energy rise of the GBFKL slope  $B_{\text{pt}}(\xi, r)$  [see Eq. (21)] and the constant nonperturbative (soft) Regge slope  $\alpha'_{\text{npt}}=0.15 \text{ GeV}^{-2}$  corresponding to the soft component of the slope  $B_{\text{npt}}(\xi, r)$  [see Eq. (18)]. As was mentioned in Ref. [18], in the energy range  $W \in (50\text{--}200) \text{ GeV}$  the effective Regge slope  $\alpha'_{\text{eff}}(\xi, r)$  varies slowly within the interval  $\sim (0.15\text{--}0.20) \text{ GeV}^{-2}$  at different scanning radii  $\leq 1 \text{ fm}$  and is approximately a flat function of the scanning radius at fixed energy corresponding to HERA experiments. For instance, at  $W=100 \text{ GeV}$ ,  $\alpha'_{\text{eff}} \sim 0.15 \text{ GeV}^{-2}$  at  $r_S \sim 0.1 \text{ fm}$ ,  $\alpha'_{\text{eff}} \sim 0.16\text{--}0.17 \text{ GeV}^{-2}$  at  $r_S \sim 0.2\text{--}0.5 \text{ fm}$ ,  $\alpha'_{\text{eff}} \sim 0.19\text{--}0.20 \text{ GeV}^{-2}$  at  $r_S \sim 0.6\text{--}0.9 \text{ fm}$ ,  $\alpha'_{\text{eff}} \geq 0.20 \text{ GeV}^{-2}$  at  $r_S \geq 1.0 \text{ fm}$ . Nonperturbative Regge slope  $\alpha'_{\text{npt}}$  only slightly modifies the overall effective Regge slope  $\alpha'$ .

In Fig. 2 we show also the energy dependence of the slope parameter for  $\rho^0$  virtual photoproduction at  $Q^2 \sim 10 \text{ GeV}^2$  vs NMC [29] and H1 [32,33] data. The growth with energy  $W$  is much smaller than at  $Q^2=0$ :  $B(\rho^0)$  rises from  $\sim 4.4 \text{ GeV}^{-2}$  at  $W=10 \text{ GeV}$  up to  $\sim 6.0 \text{ GeV}^{-2}$  at  $W=100 \text{ GeV}$ . It corresponds to the effective Regge slope  $\sim 0.17 \text{ GeV}^{-2}$ . At  $Q^2 \sim 20\text{--}30 \text{ GeV}^2$ , we predict  $\alpha' \sim 0.15 \text{ GeV}^{-2}$ , which is in accordance with value of the effective shrinkage rate of the diffraction slope for  $J/\Psi$  elastic photoproduction ( $Q^2=0$ ) presented in Ref. [11]. It confirms an approximate flavor independence of the effective Regge slope in the scaling variable  $Q^2 + m_V^2$ .

Figure 3 shows the analogical  $W$  dependence of the slope parameter for real  $\phi^0$  photoproduction together with the data from fixed target [40,41] and collider HERA experiments [42]. Unfortunately, the error bars are quite large to see a clear evidence of the shrinkage of  $B(\phi^0)$  with energy. The model predictions do not show a deviation from the data, which do not exclude the conclusion about a shrinkage of the

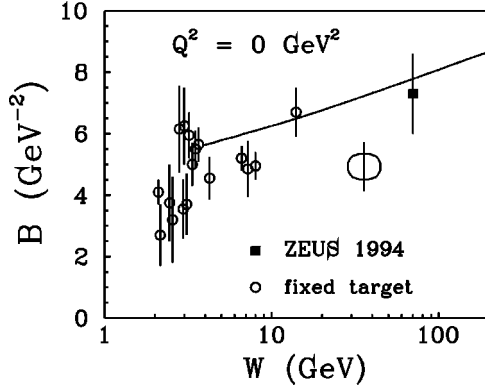


FIG. 3. The color dipole model predictions for the  $W$  dependence of the diffraction slope for the real photoproduction of  $\phi^0$  vs the low-energy fixed target [40,41] and high-energy ZEUS data [42].

diffraction peak with energy expected from the GBFKL dynamics. The energy growth of  $B(\phi^0)$  on the interval of  $W \in (10-100)$  GeV corresponds to overall effective Regge slope  $\alpha' \sim 0.20-0.21$  GeV $^{-2}$ .

Regarding a comparison of the model calculations with the data, we calculate  $B(t=0)$  as the most straightforward theoretical predictions. The data on the vector meson production correspond to a slope extracted over quite a broad range of  $t$  using an extrapolation towards  $t=0$ . The minimal value of  $t$ , which corresponds to the first experimental point in  $t$  distribution is relatively far from  $t=0$ . Also the range of  $t$  is different in different experiments. This fact explains quite a large dispersion of the low-energy data which is the most striking for  $\phi^0$  production depicted in Fig. 3 (see also Fig. 2). Because of the model calculations are at  $t=0$  and because of a well known rapid rise of the diffraction slope towards  $t=0$  [26], the experimental data may underestimate  $B(V)$  at  $t=0$ . Experimentally, the diffraction slope is extracted from the data using usually the range of  $t$ , which corresponds to average  $\langle t \rangle \sim 0.1-0.2$  GeV $^2$  and so obtained diffraction slope is smaller than  $B(t=0)$  by  $\sim 1$  GeV $^{-2}$  [26]. Therefore, for more direct comparison with the presently available experimental data instead of the directly calculated  $B(t=0)$  we report in Figs. 1–3 the value

$$B = B(t=0) - 1 \text{ GeV}^{-2}. \quad (23)$$

The uncertainties in the value of  $B$  presumably do not exceed 10% and can be reduced when more accurate data will become available. However, hereafter we will present the model predictions for the diffraction slope at  $t=0$ .

More detailed predictions for the energy and  $Q^2$  dependence of the forward diffraction slope  $B(V, t=0)$  for the  $\rho^0$  and  $\phi^0$  production [for  $(T)$ ,  $(L)$  and mixed  $(T) + \epsilon(L)$  polarizations, with  $\epsilon = 1$ ] are presented in Fig. 4. They show a substantial shrinkage of the elastic peak with energy at different  $Q^2$ . The energy rise of the diffraction slope is more evident than for production of heavy vector mesons [11].

The rate of rise with energy of the diffraction slope decreases slowly with  $Q^2$ : on the interval of the c.m.s. energy  $W \in (10-100)$  GeV the corresponding  $\alpha' \sim 0.25$  GeV $^{-2}$  at

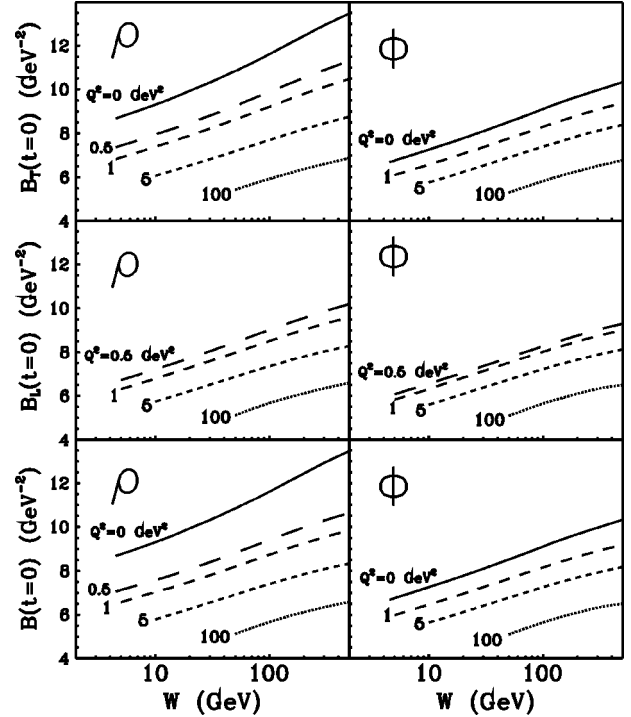


FIG. 4. The color dipole model predictions for the  $W$  dependence of the diffraction slope  $B(t=0)$  for production of transversely ( $T$ ) (top boxes), longitudinally ( $L$ ) (middle boxes) polarized, and polarization-unseparated ( $T$ ) +  $\epsilon(L)$  (bottom boxes)  $\rho^0$  and  $\phi^0$  for  $\epsilon=1$  at different values of  $Q^2$ .

$Q^2=0$ ,  $\alpha' \sim 0.21$  GeV $^{-2}$  at  $Q^2 \sim 0.5$  GeV $^2$ ,  $\alpha' \sim 0.19$  GeV $^{-2}$  at  $Q^2 \sim 1.0$  GeV $^2$ ,  $\alpha' \sim 0.17$  GeV $^{-2}$  at  $Q^2 \sim 5.0$  GeV $^2$  and  $\alpha' \sim 0.16$  GeV $^{-2}$  at  $Q^2 \sim 20$  GeV $^2$ . The effective Regge slope becomes still smaller at very large  $Q^2$  and  $W$  when the scanning radius  $r_S \leq R_c$  and the contribution of  $\alpha'_{\text{npt}} = 0.15$  GeV $^{-2}$  to the overall  $\alpha'$  becomes practically insignificant. At  $Q^2 > 100$  GeV $^2$  when the scanning radius  $r_S < R_c$ , one can observe a standard pattern of a decreasing rate of energy growth of  $B(V)$  expected from gBFKL dynamics.

The above results for the energy growth of the slope parameter can be tested using higher statistics data from HERA experiments. The measurement of energy rise of the slope parameter at different  $Q^2$  can give an information about the contribution of the nonperturbative component  $B_{\text{npt}}(\xi, r)$  to the diffraction slope and about the effective Regge slope  $\alpha'_{\text{eff}}(\xi, r)$ . The more precise data can also test the universal properties of diffraction slope and effective Regge slope for production of different vector mesons, i.e., a similarity between the production of different vector mesons when compared at the same value of the scanning radius  $r_S$  and/or the same value of  $Q^2 + m_V^2$  [see Eq. (2)].

Although new data on the diffraction slope were obtained from collider HERA experiments the present experimental information on the energy and  $Q^2$  dependence of the diffraction slope for vector meson production is still not very conclusive. Especially, it concerns  $J/\Psi$  photoproduction. There are no data yet on the diffraction slope for the real (virtual) photoproduction of  $Y$  and for the radially excited

$V'(2S)$  heavy vector mesons.<sup>2</sup> The data on the diffraction slope measuring the photoproduction and electroproduction of light vector mesons presented in Figs. 1–3 have still large error bars. The ZEUS and H1 data on virtual photoproduction give  $B(\rho^0, W \sim 80 \text{ GeV}, 7 < Q^2 < 25 \text{ GeV}^2) = 5.1 \pm 1.2 - 0.9(\text{stat}) \pm 1.0(\text{syst}) \text{ GeV}^{-2}$  [37],  $B(\rho^0, W \sim 100 \text{ GeV}, Q^2 = 28 \text{ GeV}^2) = 4.4 \pm 3.5 - 2.8(\text{stat}) + 3.7 - 1.2(\text{syst}) \text{ GeV}^{-2}$  [38] and  $B(\rho^0, W \sim 75 \text{ GeV}, Q^2 = 21.2 \text{ GeV}^2) = 4.7 \pm 1.0(\text{stat}) \pm 0.7(\text{syst}) \text{ GeV}^{-2}$  [33] which is close to  $B(J/\Psi, W = 90 \text{ GeV}, Q^2 = 0) = 4.7 \pm 1.9 \text{ GeV}^{-2}$ ,  $B(J/\Psi, W = 90 \text{ GeV}, Q^2 = 0) = 4.0 \pm 0.3 \text{ GeV}^{-2}$  from H1 data [43,44] and to  $B(J/\Psi, W = 90 \text{ GeV}, Q^2 = 0) = 4.5 \pm 1.4 \text{ GeV}^{-2}$ ,  $B(J/\Psi, W = 90 \text{ GeV}, Q^2 = 0) = 4.6 \pm 0.4(\text{stat}) + 0.4 - 0.6(\text{syst}) \text{ GeV}^{-2}$  from ZEUS data [45,46] in accordance with  $(Q^2 + m_V^2)$  scaling of the diffraction slope. High statistics data are needed from both the fixed target and the collider HERA experiments for both the exploratory study of very interesting  $Q^2$  and energy dependence of  $B(V)$  and the precise test of the  $(Q^2 + m_V^2)$  scaling of the diffraction slope.

#### IV. ANOMALOUS DIFFRACTION SLOPE IN ELECTROPRODUCTION OF 2S RADIALLY EXCITED VECTOR MESONS

The matrix element for diffractive production of radially excited  $V'(2S)$  vector mesons contains the contributions from the region of dipole sizes above and below the node position  $r_n$ . As soon as the exact node effect encounters the  $Q^2$ - and energy-dependent cancellations from the soft (large size) and hard (small size) contributions to the  $V'(2S)$  production amplitude become important.<sup>3</sup> Two main reasons affect the cancellation pattern in the diffraction slope for  $V'(2S)$  state.

First, the strong  $Q^2$  dependence of the node effect is connected with the  $Q^2$  behavior of the scanning radius  $r_S$  [see Eq. (2)]. When the scanning radius for some value of  $Q^2$  is close to  $r_n \sim R_V$  ( $R_V$  is the vector meson radius) and because of an approximate  $\sim r^2$  behavior of  $B(\xi, r)$  [18,11] even a slight variation of  $r_S$  with  $Q^2$  strongly changes the cancellation pattern and leads to an anomalous  $Q^2$  dependence of the diffraction slope.

Second, the energy dependence of the cancellations comes from a different energy dependence of the dipole cross section  $\sigma(\xi, r)$  at different dipole sizes  $r$ . Consequently, the node effect also leads to an anomalous energy dependence of the diffraction slope.

We would like to emphasize from the very beginning that the predictive power is weak and the predictions are strongly model dependent in the region of  $Q^2$  and energy when the node effect becomes exact. Presenting and discussing in this section the model predictions for the diffraction slope  $B[V'(2S)]$  we do not insist on the precise pattern of an

anomalous  $Q^2$  and energy dependence of  $B[V'(2S)]$ . We present the model calculations as an illustration of such a possible anomalous behavior of the slope parameter. We will concentrate on the production of  $V'(2S)$  light vector mesons because of a strong node effect and the fact that the new data obtained at HERA will be analyzed soon. Although in Ref. [11] the node effect has been already studied for production of  $V'(2S)$  heavy vector mesons [ $\Psi'(2S)$ ,  $Y'(2S)$ ] and a counterintuitive inequality  $B(\Psi') < B(J/\Psi)$  has been found and discussed, we will extend such an analysis also for  $V'(2S)$  light vector mesons. We will obtain a more complex pattern, which allows us to understand better the correspondence between the  $Q^2$  and energy behavior of the diffraction slope and the position of the node in  $V'(2S)$  radial wave function.

For production of  $V'(2S)$  light vector mesons the node effect depends on the polarization of the virtual photon and of the produced vector meson [10]. The wave functions of ( $T$ ) and ( $L$ ) polarized (virtual) photon are different. Different regions of  $z$  contribute to the  $\mathcal{M}_T$  and  $\mathcal{M}_L$ . Different scanning radii for production of ( $T$ ) and ( $L$ ) polarized vector mesons and different energy dependence of  $\sigma(\xi, r)$  at these scanning radii lead to a different  $Q^2$  and energy dependence of the node effect in production of ( $T$ ) and ( $L$ ) polarized  $V'(2S)$  vector mesons.

There are two possible scenarios for the node effect: the undercompensation and the overcompensation regime [16]. In the undercompensation scenario, the  $V'(2S)$  production amplitude  $\langle V'(2S) | \sigma(\xi, r) | \gamma^* \rangle$  is dominated by the positive valued contribution coming from small dipole sizes  $r \lesssim r_n$  and the  $V(1S)$  and  $V'(2S)$  photoproduction amplitudes have the same sign. This scenario corresponds, namely, to the production of  $V'(2S)$  heavy vector mesons [ $\Psi'(2S)$ ,  $Y'(2S)$ , . . .]. In the overcompensation scenario, the  $V'(2S)$  production amplitude is dominated by the negative valued contribution coming from large dipole sizes  $r \gtrsim r_n$ , and the  $V(1S)$  and  $V'(2S)$  photoproduction amplitudes have opposite sign. This scenario can correspond to the production of  $V'(2S)$  light vector mesons,  $\rho'(2S)$ ,  $\omega'(2S)$ , and  $\phi'(2S)$ .<sup>4</sup>

Anomalous properties of the diffraction slope comes namely from the expression (22). The denominator  $\mathcal{D}$  represents the well-known production amplitude. As was already mentioned, the  $V(1S)$  production amplitude is dominated by contribution from dipole size  $r \sim r_S$  (2). However, because of an approximate  $\propto r^2$  behavior of the slope parameter the integrand of the matrix element in the numerator  $\mathcal{N}$  of Eq. (22) is dominated by the dipole size  $r = r_B \sim 5/3 r_S$ .

Now let us start with a discussion about possible peculiarities in  $Q^2$  and energy dependence of the diffraction slope in a somewhat demonstrative form. Let  $\mathcal{M}_+$  and  $\mathcal{M}_-$  be the moduli of positive and negative valued contributions to the

<sup>2</sup>A more detailed discussion of the data on the slope parameter for heavy vector meson production is presented in Ref. [11].

<sup>3</sup>Manifestations of the node effect in electroproduction on nuclei were discussed earlier, see Refs. [16] and [47].

<sup>4</sup>A discussion on the experimental determination of the relative sign of the  $V'(2S)$  and  $V(1S)$  production amplitudes using the so-called Söding-Pumplin effect [48,49] has been already presented in [10].

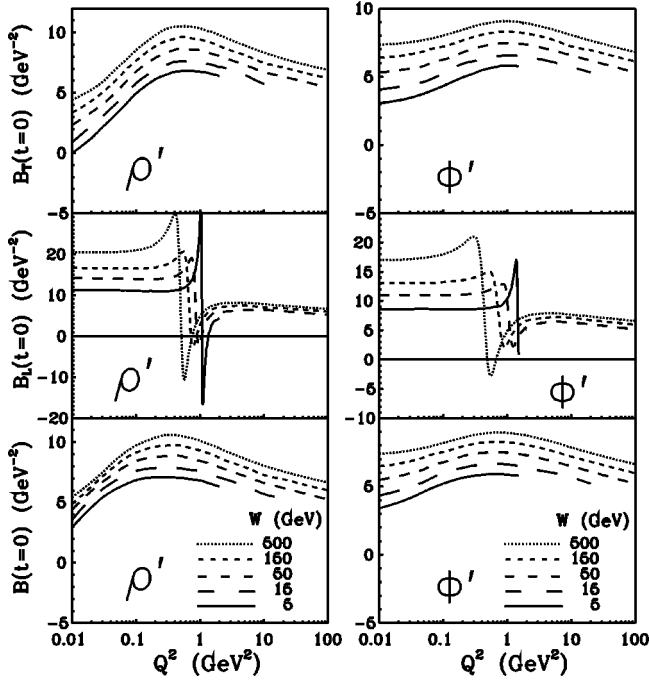


FIG. 5. The color dipole model predictions for the  $Q^2$  dependence of the diffraction slope  $B(t=0)$  for production of transversely ( $T$ ) (top boxes), longitudinally ( $L$ ) (middle boxes) polarized, and polarization-unseparated ( $T$ )+ $\epsilon(L)$  (bottom boxes)  $\rho'(2S)$  and  $\phi'(2S)$  for  $\epsilon=1$  at different values of the c.m.s. energy  $W$ .

$V'(2S)$  production amplitude from the region of dipole sizes  $r < r_n$  and  $r > r_n$ , and let  $B_+$  and  $B_-$  be the diffraction slopes for the corresponding contributions. Because of an approximate  $\sim r^2$  dependence of the diffraction slope [see Eqs. (17),(18)] we have a strong inequality

$$B_+ < B_- . \quad (24)$$

The overall  $V'(2S)$  production amplitude is  $\mathcal{M}(2S) = \mathcal{M}_+ - \mathcal{M}_-$  and the corresponding overall diffraction slope for  $V'(2S)$  production reads

$$\begin{aligned} B(2S) &= \frac{B_+ \mathcal{M}_+ - B_- \mathcal{M}_-}{\mathcal{M}_+ - \mathcal{M}_-} \\ &= B_+ - (B_- - B_+) \frac{\mathcal{M}_-}{\mathcal{M}_+ - \mathcal{M}_-} , \end{aligned} \quad (25)$$

which can be rewritten in a more convenient form for the following discussion:

$$B(2S) - B(1S) = -(B_- - B_+) \frac{\mathcal{M}_-}{\mathcal{M}_+ - \mathcal{M}_-} , \quad (26)$$

where  $B(1S) \approx B_+$  for production of  $V(1S)$  vector mesons. For the diffractive production of  $V'(2S)$  heavy vector mesons the production amplitude  $\mathcal{M}(2S)$  is positive valued (undercompensation scenario) at  $Q^2=0$  and consequently we predict from Eq. (26) a counterintuitive inequality  $B[\Psi'(2S)] < B[J/\Psi(1S)]$  [11] although the rms radius of

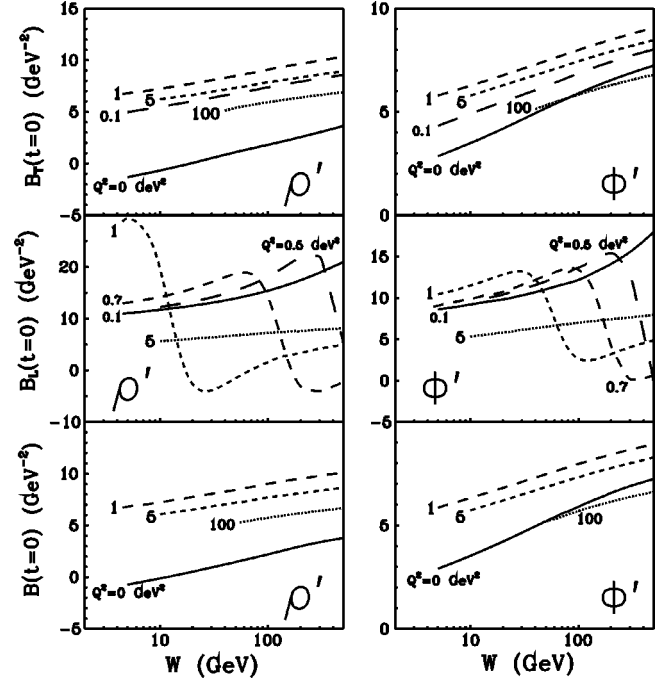


FIG. 6. The color dipole model predictions for the  $W$  dependence of the diffraction slope  $B(t=0)$  for production of transversely ( $T$ ) (top boxes), longitudinally ( $L$ ) (middle boxes) polarized, and polarization-unseparated ( $T$ )+ $\epsilon(L)$  (bottom boxes)  $\rho'(2S)$  and  $\phi'(2S)$  for  $\epsilon=1$  at different values of  $Q^2$ .

$\Psi'$  is much larger than  $R_{J/\Psi}$ . However, as we will manifest below, this is not always true in production of  $V'(2S)$  light vector mesons.

### Undercompensation scenario

The undercompensation scenario [denominator in Eq. (22) is positive valued,  $\mathcal{D} > 0$ ] corresponds to the production of ( $T$ ) polarized  $\rho'(2S)$  and  $\phi'(2S)$  at  $Q^2=0$  using the vector meson wave functions from Ref. [10]. Because of  $r_B > r_S$ , there are two possibilities concerning the sign of the matrix element  $\mathcal{N}$  in Eq. (22).

(i)  $\mathcal{N} < 0$ :  $\mathcal{N}$  and  $\mathcal{D}$  have the opposite sign. Consequently, the diffraction slope in the photoproduction limit is negative valued. This pattern corresponds to diffractive photoproduction of  $\rho'_T(2S)$  at small energy (see Figs. 5 and 6—top boxes).

(ii)  $\mathcal{N} > 0$ :  $\mathcal{N}$  and  $\mathcal{D}$  have the same sign. Consequently, the diffraction slope in the photoproduction limit is positive valued. This pattern corresponds to diffractive photoproduction of  $\phi'_T(2S)$  (see Figs. 5 and 6—top boxes) and the node effect is weaker in comparison with  $\rho'_T(2S)$  photoproduction.

In both cases we predict from Eq. (26) the counterintuitive inequalities  $B[\rho'_T(2S)] < B[\rho_T(1S)]$  and  $B[\phi'_T(2S)] < B[\phi_T(1S)]$  (compare Figs. 4 and 5—top boxes), which are analogical to that for charmonium diffractive photoproduction [11]. The stronger is the node effect the smaller is the  $V'(2S)$  forward diffraction slope at  $Q^2=0$  and the larger is the difference  $|B(2S) - B(1S)|$ .

A decrease of the scanning radius with  $Q^2$  leads to a very rapid decrease of the negative valued contribution to the diffraction slope coming from  $r \geq r_n$  and consequently leads to a steep rise of  $B[V_T'(2S)]$  with  $Q^2$ . The higher is  $Q^2$  the weaker is the node effect and the smaller is the difference  $|B(2S) - B(1S)|$ . However, the inequalities  $B[\rho_T'(2S)] < B[\rho_T(1S)]$  and  $B[\phi_T'(2S)] < B[\phi_T(1S)]$  are still kept. Because of a stronger node effect for  $\rho_T'(2S)$  production we predict a steeper rise with  $Q^2$  of the slope parameter for  $\rho_T'(2S)$  than for  $\phi_T'(2S)$  production.

At still larger  $Q^2$  and at fixed energy the slope parameter  $B[V_T'(2S)]$  has a broad maximum at some value of  $Q^2 \sim Q_T^2 \in (0.5 - 2.0)$  GeV<sup>2</sup>. At very large  $Q^2 \gg m_V^2$  when the node effect becomes negligible,  $B(2S) \sim B(1S)$  and  $B[V_T'(2S)]$  decreases monotonously with  $Q^2$  following the  $Q^2$  dependence of  $B[V_{L,T}(1S)]$  for ground state vector mesons (see Fig. 4).

The above described pattern of nonmonotonic  $Q^2$  dependence of the diffraction slope is depicted in Fig. 5 (bottom boxes) for both the  $\rho_T'(2S)$  and  $\phi_T'(2S)$  production, where we present the model predictions for the forward diffraction slope ( $t=0$ ) as a function of  $Q^2$  at different values of the c.m.s. energy  $W$ .

#### Overcompensation scenario

The overcompensation scenario [denominator in Eq. (22) is negative valued,  $\mathcal{D} < 0$ ], corresponds to the production of ( $L$ ) polarized  $\rho'(2S)$  and  $\phi'(2S)$  at  $Q^2=0$  using the vector meson wave functions from Ref. [10]. Because of  $r_B > r_S$ , the matrix element  $\mathcal{N}$  in Eq. (22) is safely negative valued, i.e.,  $\mathcal{N} < 0$  and has the same sign as  $\mathcal{D}$ . Consequently, the diffraction slope in the photoproduction limit is positive valued as it can be also in the undercompensation regime described above. The sign of the diffraction slope  $B(2S)$  at  $Q^2=0$  cannot distinguish between the overcompensation and undercompensation scenarios. However, because of  $\mathcal{M}(2S) < 0$  the difference  $B(2S) - B(1S)$  is positive valued as it follows from Eq. (26). As the result we predict the expected inequalities (reverse inequalities in comparison with the undercompensation scenario)  $B[\rho_L(1S)] < B[\rho_L'(2S)]$  and  $B[\phi_L(1S)] < B[\phi_L'(2S)]$ , what is a new result in comparison with the color dipole predictions for heavy vector mesons presented in the paper [11].

With the decrease of the scanning radius with  $Q^2$  there is a rapid decrease of the negative contributions to  $\mathcal{N}$  and  $\mathcal{D}$  coming from  $r \geq r_n$ . For some  $Q^2 \sim Q_L'^2 \in (0.5 - 1.5)$  GeV<sup>2</sup> one encounters the exact node effect first for the denominator  $\mathcal{D}$  and  $B[V_L'(2S)]$  has a peak for both the  $\rho_L'(2S)$  and  $\phi_L'(2S)$  production. The value of  $B[V_L'(2S)]$  corresponding to this exact node effect will be finite due to a different node effect for the real and imaginary part of the production amplitude. The onset of the node effect causes also the rapid continuous transition of  $B[V_L'(2S)]$  from positive to negative values when the matrix element  $\mathcal{D}$  passes from the overcompensation to undercompensation regime. Consequently, for  $Q^2 > Q_L'^2$ ,  $\mathcal{D} > 0$ ,  $\mathcal{N}$  is kept to be negative valued and  $B[V_L'(2S)]$  starts to rise from its minimal negative value

(see Fig. 5—middle boxes).<sup>5</sup> At still larger  $Q^2$  the following pattern of the  $Q^2$  behavior of  $B[V_L'(2S)]$  is analogical to that for  $Q^2$  dependence of  $B[V_T'(2S)]$ . We find again a broad maxima of  $B[V_L'(2S)]$  at  $Q^2 \sim Q_L'^2 \in (2.0 - 5.0)$  GeV<sup>2</sup>. This pattern of nonmonotonic  $Q^2$  dependence of the diffraction slope is depicted in Fig. 5 (middle boxes) for both the  $\rho_L'(2S)$  and  $\phi_L'(2S)$  production and can be tested at HERA. For the production of polarization unseparated  $V'(2S)$ , the anomalous properties of  $B[V_L'(2S)]$  are essentially invisible and the corresponding slope parameter  $B[V'(2S)]$  has an analogical  $Q^2$  dependence as  $B[V_T'(2S)]$  and is shown in Fig. 5 (bottom boxes).

The predicted pattern of nonmonotonic  $Q^2$  dependence of the diffraction slope for production of ( $T$ ), ( $L$ ) polarized and polarization unseparated  $\rho'(2S)$  and  $\phi'(2S)$  is strikingly different from a monotonic  $Q^2$  behavior of the slope parameter for  $V(1S)$  production (see Fig. 4). Here we cannot insist on the precise value of  $Q_L'^2$  which is a subject of the soft-hard cancellations. We would like only to emphasize that the exact node effect for  $B[V_L'(2S)]$  is at a finite  $Q_L'^2$ .

To conclude the  $Q^2$  dependence of  $B(2S)$ , the undercompensation scenario is characterized by a broad maximum at  $Q^2 \sim Q_T^2$  and can be tested experimentally at HERA measuring the virtual photoproduction of the  $\rho'(2S)$  and  $\phi'(2S)$  at  $Q^2 \in (0 - 10)$  GeV<sup>2</sup> and at different values of energy. However, the overcompensation scenario is manifested by a sharp peak followed by a very rapid transition of the diffraction slope from positive to negative values (see discussion in footnote) at  $Q^2 \sim Q_L'^2$  and then by a broad maximum at  $Q^2 \sim Q_L'^2$  and can be also investigated at HERA separating ( $L$ ) polarized  $\rho_L'(2S)$  and  $\phi_L'(2S)$  at moderate  $Q^2 \in (0.1 - 5.0)$  GeV<sup>2</sup>. Here we would like to emphasize that only the experiment can help in decision between the undercompensation and overcompensation scenarios.

The energy dependence of the slope parameter  $B[V'(2S)]$  at different  $Q^2$  is shown in Fig. 6 and has its own peculiarities. Let us start with  $B[V_T'(2S)]$  at  $Q^2=0$  when the production amplitude is in the undercompensation regime,  $\mathcal{D} > 0$ . Figure 6 demonstrates (top boxes) the steeper rise with energy of the diffraction slope at lower  $Q^2$ . There are several reasons for such a behavior. First, the GBFKL dynamics predicts a steeper rise with energy of the positive contribution to the amplitudes  $\mathcal{N}$  and  $\mathcal{D}$  coming from small size dipoles  $r \leq r_n$  than the negative contribution coming from large size dipoles  $r \geq r_n$ . Consequently, the destructive interference of these two contributions is weaker at higher energy. Second, at  $Q^2=0$  the amplitudes  $\mathcal{N}$  and  $\mathcal{D}$  in Eq. (22) have different corresponding scanning radii,  $r_B > r_S$ . Third, the energy dependence of the slope parameter is given

<sup>5</sup>For production of  $\phi_L'(2S)$  vector mesons the diffraction slope does not reach the negative values at small and moderate energies after its continuous transition when the node effect was encountered for  $\mathcal{D}$  because the node effect is immediately encountered for  $\mathcal{N}$  also. This fact also concerns the energy dependence of the diffraction slope.

by the effective Regge slope  $\alpha'$  [see Eqs. (18) and (21)], which decreases with  $Q^2$ . Consequently, for  $\rho_T'(2S)$  production the above destructive interference in  $\mathcal{N}$  decreases drastically with  $W$  the negative contribution from  $r \geq r_n$  until the exact node effect is reached, i.e.,  $B[V_T'(2S)] = 0$ , and the undercompensation scenario also for the numerator (i.e.,  $\mathcal{N} > 0$ ) starts to be realized at  $W \sim 20$  GeV.<sup>6</sup> However, closeness of the scanning radius to the node position in  $\mathcal{N}$  leads to a somewhat steeper growth with energy of  $B[V_T'(2S)]$  than the expected energy rise coming only from the effective Regge slope. For example, for  $\rho_T'(2S)$  production we predict the rise of  $B[V_T'(2S)]$  by  $\sim 2.8$  GeV<sup>-2</sup>, from  $W = 10$  to  $W = 100$  GeV. At  $Q^2 \geq 1.0$  GeV<sup>2</sup> when both  $\mathcal{N}$  and  $\mathcal{D}$  are in the undercompensation regime and the node effect becomes weaker, the energy growth of  $B[V'(2S)]$  is connected mainly with the effective Regge slope and we predict approximately the same quantities and energy growth for  $B[V'(2S)]$  and  $B[V(1S)]$  (compare Figs. 4 and 6).

The successful separation of the ( $L$ ) polarized  $V_L'(2S)$  mesons at HERA offers an unique possibility to study an anomalous  $Q^2$  and energy dependence of the diffraction slope connected with the overcompensation scenario. At  $Q^2 = 0$  we have the onset of the overcompensation scenario for both the matrix elements  $\mathcal{N}$  and  $\mathcal{D}$  of Eq. (22). At moderate energy and  $Q^2$  close but smaller than  $Q_L'^2$ , the negative valued contribution coming from  $r \geq r_n$  still takes over in  $\mathcal{D}$  ( $\mathcal{N} < 0$  is safely in the overcompensation regime due to  $r_B > r_S$ ). Because of a steeper rise with energy of the positive contribution to the  $V'(2S)$  production amplitude coming from  $r \leq r_n$  than the negative contribution from  $r \geq r_n$ , we find an exact cancellation of these two contributions to  $\mathcal{D}$  and a maximum of the diffraction slope  $B[V_L'(2S)]$  at some intermediate energy followed by its rapid continuous transition from the positive to negative values, when  $\mathcal{D}$  passes from the overcompensation to the undercompensation regime. Different node effects for the real and imaginary part of the production amplitude provides such a continuous transition. At larger energies  $\mathcal{D} > 0$  (undercompensation regime) and consequently  $B[V_L'(2S)]$  is negative valued and starts to rise from its minimal negative value [see discussion in the footnote for  $\phi_L'(2S)$  production]. Such a situation is depicted in Fig. 6 (middle boxes), where we predict with the wave functions from Ref. [10] a nonmonotonic energy behavior of  $B[V_L'(2S)]$  for both  $\rho'(2S)$  and  $\phi'(2S)$  production at  $Q^2 \sim Q_L'^2$ . The position of the maximum  $W_i$  and the transition from the positive to negative values of  $B[V_L'(2S)]$  depends on  $Q^2$ . For example, at  $Q^2 \sim 0.7$  GeV<sup>2</sup>, we find  $W_i \sim 70$ – $80$  GeV. The position of  $W_i$  is shifted towards smaller values of  $W$  at larger  $Q^2$  and can be measured at HERA.

At higher  $Q^2$  and smaller scanning radii, the further pattern of the energy behavior for  $B[V_L'(2S)]$  is analogical to that for  $B[V_T'(2S)]$ . At still larger  $Q^2$ , after the exact node

effect was also reached in  $\mathcal{N}$  at  $Q^2 \sim Q_L'^2 > Q_L'^2$ , both  $\mathcal{N}$  and  $\mathcal{D}$  are in the undercompensation regime. At very large  $Q^2$ , the node effect also in  $\mathcal{N}$  is weaker and the energy growth of  $B[V_L'(2S)]$  is controlled practically by the effective Regge slope. As the result we predict again almost the same quantities and energy growth for  $B[V_L'(2S)]$  and  $B[V_L(1S)]$ .

If ( $T$ ) and ( $L$ ) polarized  $V_T'(2S)$  and  $V_L'(2S)$  mesons will be separated experimentally there is a chance for experimental determination of a concrete scenario in ( $T$ ) and ( $L$ ) polarized  $V'(2S)$  production amplitude. The simplest test can be realized in the photoproduction limit ( $Q^2 = 0$ ) for a broad energy range. If the data will report the counterintuitive inequality  $B(2S) < B(1S)$  [ $B(2S)$  can also be negative valued] then  $V'(2S)$  production amplitude is in the undercompensation regime (positive valued). In the opposite case when the expected inequality  $B(2S) > B(1S)$  will be obtained from the data then  $V'(2S)$  production amplitude is in the overcompensation regime (negative valued). For the production of ( $L$ ) polarized vector mesons the values of  $Q^2$  should be high enough to have the data with a reasonable statistics, however, must not be very large in order to have a strong node effect. We propose the range of  $Q^2 \in (0.5 - 5.0)$  GeV<sup>2</sup> for the exploratory study of the overcompensation scenario at HERA.

## V. CONCLUSIONS

We study the forward diffraction slope for diffractive photo- and electroproduction of ground state  $V(1S)$  and radially excited  $V'(2S)$  light vector mesons in the framework of the color dipole GBFKL dynamics. In this dynamics the energy dependence of the  $V(1S)$  vector meson production is controlled by the energy dependence of the dipole cross section which is steeper for smaller dipole sizes. The energy dependence of the diffraction slope for  $V(1S)$  production is given by the effective Regge slope with a small variation with energy. The  $Q^2$  dependence of the  $V(1S)$  vector meson production is controlled by the shrinkage of the transverse size of the virtual photon and by the dipole size dependence of the color dipole cross section. The  $Q^2$  behavior of the diffraction slope is given by an approximate geometrical contribution  $\sim r^2$ , which is related with  $Q^2$  through the scanning radius (2). We present for the first time a reach pattern of  $Q^2$  and energy dependence of the diffraction slope for  $\rho^\circ$  and  $\phi^\circ$  production and find a substantial growth (by  $\sim 2.3$ – $2.4$  GeV<sup>-2</sup> for  $\rho^\circ$  production and by  $\sim 1.9$ – $2.0$  GeV<sup>-2</sup> for  $\phi^\circ$  production) of the slope parameter from the fixed target ( $W \sim 10$ – $15$  GeV) to the collider HERA ( $W \sim 100$ – $150$  GeV) range of energy. The shrinkage with energy of the diffraction slope is weaker at larger values of  $Q^2$  and the corresponding shrinkage rate decreases also with  $m_V$  in accordance with the GBFKL dynamics. The model predictions for the diffraction slope for the  $\rho^\circ$  and  $\phi^\circ$  production are in agreement with the data from the fixed target (CHIO, NMC) and collider HERA (H1, ZEUS) experiments. However, the relatively large error bars of the data preclude any definite statement about a shrinkage of the slope parameter with energy. The data show also a trend to smaller values of

<sup>6</sup>For production of  $\phi_L'(2S)$  vector mesons the matrix element  $\mathcal{N} > 0$  already at  $Q^2 = 0$  and at small energy resulting in positive valued diffraction slope.

the diffraction slope as  $Q^2$  increases in agreement with the GBFKL dynamics. We analyze from the available data the universality properties of the diffraction slope as a function of the scaling variable  $Q^2 + m_V^2$ .

The second class of predictions is related to the diffraction slope for the production of  $V'(2S)$  vector mesons. A detailed analysis of a very complicated pattern of anomalous  $Q^2$  and energy behavior of the slope parameter for production of radially excited light vector mesons is presented here for the first time and completes the previous analysis for heavy vector mesons published in Ref. [11]. As a consequence of the strong node effect in electroproduction of  $\rho'(2S)$  and  $\phi'(2S)$  we present a strikingly different  $Q^2$  and energy dependence of the forward diffraction slopes  $B[V'(2S)]$  and  $B[V(1S)]$ . At moderate energies, we find a nonmonotonic  $Q^2$  dependence of the slope parameter which can be tested at HERA in the range of  $Q^2 \in (0-10)$  GeV<sup>2</sup>. For the production of (*L*) polarized  $V'(2S)$  mesons we find a plausible overcompensation scenario leading to a sharp peak followed immediately by a very rapid transition of the slope

parameter from positive to negative values at  $Q^2 \sim Q_L'^2 \in (0.5-1.5)$  GeV<sup>2</sup>. The position of this rapid transition  $Q_L'^2$  is energy dependent and leads to a nonmonotonic energy dependence of  $B[V_L'(2S)]$  at fixed  $Q^2$ . At  $Q^2=0$  when the node effect is strong, for the undercompensation scenario we predict an analogical counterintuitive inequality as for heavy vector mesons  $B[V'(2S)] < B[V(1S)]$ . However, for the overcompensation scenario we predict the expected standard inequality  $B[V'(2S)] > B[V(1S)]$ . This is a very crucial point of a possible experimental determination of a concrete scenario (and the position of the node as well) extracting from the data at HERA the diffraction slope at  $t=0$  for the production of  $V'(2S)$  mesons in the photoproduction limit.

At larger  $Q^2$  and/or shorter scanning radius the node effect becomes weak and we predict for  $V'(2S)$  mesons the standard monotonic  $Q^2$  and energy dependence of the slope parameter as for  $V(1S)$  mesons. One needs more accurate data from both the fixed target and collider HERA experiments for the exploratory study of  $Q^2$  and energy dependence of the diffraction slopes  $B[V'(2S)]$  and  $B[V(1S)]$ .

- 
- [1] A. Donnachie and P. V. Landshoff, Phys. Lett. B **185**, 403 (1987); J. R. Cuddell, Nucl. Phys. **B336**, 1 (1990).
- [2] B. Z. Kopeliovich and B. G. Zakharov, Phys. Rev. D **44**, 3466 (1991).
- [3] M. G. Ryskin, Z. Phys. C **57**, 89 (1993).
- [4] B. Z. Kopeliovich, J. Nemchik, N. N. Nikolaev, and B. G. Zakharov, Phys. Lett. B **309**, 179 (1993).
- [5] B. Z. Kopeliovich, J. Nemchik, N. N. Nikolaev, and B. G. Zakharov, Phys. Lett. B **324**, 469 (1994).
- [6] J. Nemchik, N. N. Nikolaev, and B. G. Zakharov, Phys. Lett. B **341**, 228 (1994).
- [7] S. J. Brodsky *et al.*, Phys. Rev. D **50**, 3134 (1994).
- [8] J. R. Forshaw and M. G. Ryskin, Z. Phys. C **68**, 137 (1995).
- [9] E. Gotsman, E. M. Levin, and U. Maor, Nucl. Phys. **B464**, 251 (1996).
- [10] J. Nemchik, N. N. Nikolaev, E. Predazzi, and B. G. Zakharov, Z. Phys. C **75**, 71 (1997).
- [11] J. Nemchik, N. N. Nikolaev, E. Predazzi, B. G. Zakharov, and V. R. Zoller, Zh. Éksp. Teor. Fiz. **113**, 1930 (1998) [JETP **86**, 1054 (1998)].
- [12] N. N. Nikolaev and B. G. Zakharov, Z. Phys. C **49**, 607 (1991); **53**, 331 (1992).
- [13] N. Nikolaev and B. G. Zakharov, Zh. Éksp. Teor. Fiz. **105**, 1117 (1994) [JETP **78**, 598 (1994)]; Z. Phys. C **64**, 631 (1994).
- [14] N. N. Nikolaev, B. G. Zakharov, and V. R. Zoller, Pis'ma Zh. Éksp. Teor. Fiz. **59**, 8 (1994) [JETP Lett. **59**, 6 (1994)]; Zh. Éksp. Teor. Fiz. **105**, 1606 (1994) [JETP **78**, 865 (1994)]; Phys. Lett. B **328**, 486 (1994).
- [15] N. N. Nikolaev, Comments Nucl. Part. Phys. **21**, 41 (1992).
- [16] J. Nemchik, N. N. Nikolaev, and B. G. Zakharov, Phys. Lett. B **339**, 194 (1994).
- [17] J. Nemchik, Eur. Phys. J. C (to be published), hep-ph/0003244.
- [18] N. N. Nikolaev, B. G. Zakharov, and V. R. Zoller, Phys. Lett. B **366**, 337 (1996).
- [19] N. N. Nikolaev, B. G. Zakharov, and V. R. Zoller, Pis'ma Zh. Éksp. Teor. Fiz. **60**, 678 (1994) [JETP Lett. **60**, 694 (1994)].
- [20] J. B. Kogut and D. E. Soper, Phys. Rev. D **1**, 2901 (1970).
- [21] V. N. Gribov and A. A. Migdal, Yad. Fiz. **8**, 1213 (1968) [Sov. J. Nucl. Phys. **8**, 703 (1969)].
- [22] N. N. Nikolaev and B. G. Zakharov, Phys. Lett. B **327**, 149 (1994).
- [23] H1 Collaboration, I. Abt *et al.*, Nucl. Phys. **B407**, 515 (1993).
- [24] ZEUS Collaboration, M. Derrick *et al.*, Phys. Lett. B **316**, 412 (1993).
- [25] J. Nemchik, N. N. Nikolaev, E. Predazzi, and B. G. Zakharov, Phys. Lett. B **374**, 199 (1996).
- [26] A. Schiz *et al.*, Phys. Rev. D **24**, 26 (1981); J. P. Burq *et al.*, Phys. Lett. **109B**, 111 (1982).
- [27] J. Nemchik, Phys. Lett. B **497**, 235 (2001).
- [28] CHIO Collaboration, W. D. Shambroom *et al.*, Phys. Rev. D **26**, 1 (1982).
- [29] NMC Collaboration, M. Arneodo *et al.*, Nucl. Phys. **B429**, 503 (1994).
- [30] E665 Collaboration, M. R. Adams *et al.*, Z. Phys. C **74**, 237 (1997).
- [31] H1 Collaboration, S. Aid *et al.*, Nucl. Phys. **B463**, 3 (1996).
- [32] H1 Collaboration, T. Ahmed *et al.*, "Exclusive  $\rho^0$  Production in Deep-inelastic Scattering Events at HERA," presented at the International Europhysics Conference on HEP, Brussels, 1995, paper No. EPS-0490; H1 Collaboration, S. Aid *et al.*, Nucl. Phys. **B468**, 3 (1996).
- [33] H1 Collaboration, C. Adloff *et al.*, Eur. Phys. J. C **13**, 371 (2000).
- [34] ZEUS Collaboration, M. Derrick *et al.*, Z. Phys. C **69**, 39 (1995).
- [35] ZEUS Collaboration, J. Breitweg *et al.*, Z. Phys. C **73**, 253 (1997).
- [36] ZEUS Collaboration, J. Breitweg *et al.*, Eur. Phys. J. C **2**, 247 (1998).

- [37] ZEUS Collaboration, M. Derrick *et al.*, Phys. Lett. B **356**, 601 (1995).
- [38] ZEUS Collaboration, J. Breitweg *et al.*, Eur. Phys. J. C **6**, 603 (1999).
- [39] W. G. Jones *et al.*, Phys. Rev. Lett. **21**, 586 (1968); C. Berger *et al.*, Phys. Lett. **39B**, 659 (1972); SBT Collaboration, J. Ballam *et al.*, Phys. Rev. D **5**, 545 (1972); G. E. Gladding *et al.*, *ibid.* **8**, 3721 (1973); OMEGA Photon Collaboration, D. Aston *et al.*, Nucl. Phys. **B209**, 56 (1982).
- [40] J. Busenitz *et al.*, Phys. Rev. D **40**, 1 (1989), and references therein.
- [41] R. Erbe *et al.*, Phys. Rev. **175**, 1669 (1968); Berger [39]; J. Ballam *et al.*, Phys. Rev. D **7**, 3150 (1973); H. J. Bersh *et al.*, Nucl. Phys. **B70**, 257 (1974); H. J. Behrend *et al.*, Phys. Lett. **56B**, 408 (1975); D. P. Barber *et al.*, *ibid.* **79B**, 150 (1978); D. Aston *et al.*, Nucl. Phys. **B172**, 1 (1980); M. Atkinson *et al.*, Z. Phys. C **27**, 233 (1985).
- [42] ZEUS Collaboration, M. Derrick *et al.*, “Elastic Photoproduction of  $\omega$ ,  $\phi$  and  $\rho'$  mesons at HERA,” presented at the International Europhysics Conference on HEP, Brussels, 1995, paper EPS-0389; Phys. Lett. B **377**, 259 (1996).
- [43] H1 Collaboration, T. Ahmed *et al.*, Phys. Lett. B **338**, 507 (1994).
- [44] H1 Collaboration, T. Ahmed *et al.*, Nucl. Phys. **B472**, 3 (1996).
- [45] ZEUS Collaboration, M. Derrick *et al.*, Phys. Lett. B **350**, 120 (1995).
- [46] ZEUS Collaboration, J. Breitweg *et al.*, Z. Phys. C **75**, 215 (1997).
- [47] O. Benhar *et al.*, Phys. Rev. Lett. **74**, 3565 (1995); O. Benhar *et al.*, Zh. Éksp. Teor. Fiz. **111**, 769 (1997) [JETP **84**, 421 (1997)].
- [48] P. Söding, Phys. Lett. **19**, 702 (1966).
- [49] J. Pumplin, Phys. Rev. D **2**, 1859 (1970).